Dynamics of liquid rope coiling

Mehdi Habibi
Institute for Advanced Studies in Basic Sciences, Zanjan 45195-1159, Iran and Laboratoire de Physique Statistique, UMR 8550 CNRS, École Normale Supérieure, 24, rue Lhomond, 75231 Paris Cedex 05, France

Maniya Maleki
Institute for Advanced Studies in Basic Sciences, Zanjan 45195-1159, Iran

Ramin Golestanian
Institute for Advanced Studies in Basic Sciences, Zanjan 45195-1159, Iran and Department of Physics and Astronomy, University of Sheffield, Sheffield S3 7RH, United Kingdom

Neil M. Ribe
Laboratoire de Dynamique des Systèmes Géologiques, Institut de Physique du Globe de Paris, UMR 7154 CNRS, 4, place Jussieu, 75252 Paris cédex 05, France

Daniel Bonn
Laboratoire de Physique Statistique, UMR 8550 CNRS, École Normale Supérieure, 24, rue Lhomond, 75231 Paris Cedex 05, France and Van der Waals-Zeeman Institute, University of Amsterdam, Valckenierstraat 65, 1018 XE Amsterdam, the Netherlands
(Received 24 July 2006; published 11 December 2006)

We present a combined experimental and numerical investigation of the coiling of a liquid "rope" falling on a solid surface, focusing on three little-explored aspects of the phenomenon: The time dependence of "inertio-gravitational" coiling, the systematic dependence of the radii of the coil and the rope on the experimental parameters, and the "secondary buckling" of the columnar structure generated by high-frequency coiling. Inertio-gravitational coiling is characterized by oscillations between states with different frequencies, and we present experimental observations of four distinct branches of such states in the frequency-fall height space. The transitions between coexisting states have no characteristic period, may take place with or without a change in the sense of rotation, and usually (but not always) occur via an intermediate "figure of eight" state. We present extensive laboratory measurements of the radii of the coil and of the rope within it, and show that they agree well with the predictions of a "slender-rope" numerical model. Finally, we use dimensional analysis to reveal a systematic variation of the critical column height for secondary buckling as a function of (dimensionless) flow rate and surface tension parameters.

DOI: 10.1103/PhysRevE.74.066306 PACS number(s): 47.20.Gv, 47.20.Bp

I. INTRODUCTION

A thin stream of honey poured from a sufficient height onto toast forms a regular helical corkscrew or "coil." This instability was first investigated experimentally by Barnes and Woodcock [1], who called it "liquid rope coiling" by analogy to the coiling of an elastic rope. However, elastic rope coiling is difficult to study experimentally, both because the frictional contact of the rope with a solid surface is hard to control and because the natural (unstressed) state of most elastic ropes is not perfectly straight. This is probably why no experiments on elastic rope coiling have (to our knowledge) been published, while many have been reported for the coiling of liquid ropes [1–5,7–10]. The first theoretical study of liquid rope coiling was undertaken by Taylor [11], who suggested that the instability is similar to the buckling instability of an elastic rod (or solid rope) under an applied compressive stress. Subsequent theoretical studies based on linear stability analysis determined the critical fall height and frequency of incipient coiling [12,13]. More recently, Mahadevan *et al.* [8] experimentally measured coiling frequencies in the high frequency or "inertial" limit, and showed [14] that they obey a scaling law involving a balance between rotational inertia and the viscous forces that resist the bending of the rope.

This behavior however is just one among several that are possible for liquid ropes. Ribe [15] proposed a numerical model for coiling based on an asymptotic "slender rope" theory, and solved the resulting equations using a numerical continuation method. The solutions showed that three distinct coiling regimes (viscous, gravitational, and inertial) can exist depending on the relative magnitudes of the viscous, gravitational, and inertial forces acting on the rope, and that the coiling frequency can be multivalued at a fixed fall height within a certain range. Maleki *et al.* [9] reported experimental measurements of the coiling frequency of different silicone oils in all three regimes that agreed quantitatively with the numerical predictions, including the multivaluedness. The multivalued regime was subsequently investigated in more detail by Ribe *et al.* [10] using both laboratory experiments and the slender-rope numerical model. They found that multivalued coiling corresponds to a distinct "inertio-gravitational" regime in which the rope behaves as a distributed pendulum with a discrete spectrum of eigenfrequencies. Comparison of the numerics with experimental measurements showed that some of the numerically

predicted branches of the curve of coiling frequency vs height are experimentally accessible while others are not, thereby accounting for the experimental observation of abrupt transitions between different coiling frequencies [9].

Here we present a more complete laboratory investigation of liquid rope coiling, focusing on three aspects of the phenomenon that have not previously been studied. First, we examine in detail the time dependence of multivalued (inertio-gravitational) coiling. For a given set of experimental conditions, we observe four distinct branches in the curve of frequency vs height, in agreement with the numerical predictions. We further find that transitions between low- and high-frequency branches occur chaotically, without any characteristic frequency and with changes in the sense of rotation that appear to be random. Second, we present extensive measurements of the radii of the rope within the coil and of the coil itself as functions of the flow rate, the fluid viscosity, and the fall height, and compare these with the predictions of the slender-rope model. Finally, we explore the "secondary buckling" instability that occurs when the coil formed by high-frequency (inertial) coiling buckles under its own weight upon exceeding a critical height. We use dimensional analysis to document the systematic dependence of the critical height on the flow rate and on the surface tension of the fluid.

II. EXPERIMENTAL PROCEDURE

We used two different experimental setups for low-frequency and high-frequency experiments. In both cases, silicone oil with density $\rho=0.97$ g cm^{-3}, surface tension coefficient $\gamma=21.5$ dyn cm^{-1}, and (variable) kinematic viscosity ν was injected at a volumetric rate Q from a hole of diameter $d\equiv 2a_0$ and subsequently fell a distance H onto a glass plate. Movies of the coiling experiments are available [6].

Figure 1 shows the setup for low-frequency coiling, in which silicone oils with $\nu=125$, 300, or 1000 cm^2 s^{-1} were extruded from a syringe by a piston driven by a computer-controlled stepper motor. This arrangement allowed access to the very low flow rates required to observe both low-frequency "viscous" coiling and multivalued "inertio-gravitational" coiling with more than two distinct branches. The flow rate was measured to within 10^{-4} ml s^{-1} by recording the volume of fluid in the syringe as a function of time. A CCD camera operating at 25 frames s^{-1} was used to make movies, from which the coiling frequency was measured by frame counting. The radius of the rope and the fall height (especially for small fall heights) were measured on the still images to within 0.02 and 0.2 mm, respectively. For large heights we used a ruler to determine H to within 1 mm.

In the setup used to study high-frequency coiling (Fig. 2), silicone oil with viscosity $\nu=300$ cm^2 s^{-1} fell freely from a hole of radius $a_0=0.25$ cm at the bottom of a reservoir. To maintain a constant flow rate Q, the reservoir was made to overflow continually by the addition of silicone oil from a second beaker. Three series of experiments were performed with flow rates $Q=0.085$, 0.094, and 0.104 cm^3 s^{-1} and fall heights $2.0\ \text{cm}\leqslant H\leqslant 49.4$ cm. The coiling frequency was measured by frame counting on movies taken with a high speed camera operating at 125–1000 frames s^{-1}, depending on the temporal resolution required. The flow rate was measured to within 1% by weighing the amount of oil on the plate as a function of time during the experiment. The radius a_1 of the rope just above the coil was measured from still pictures taken with a high resolution Nikon digital camera

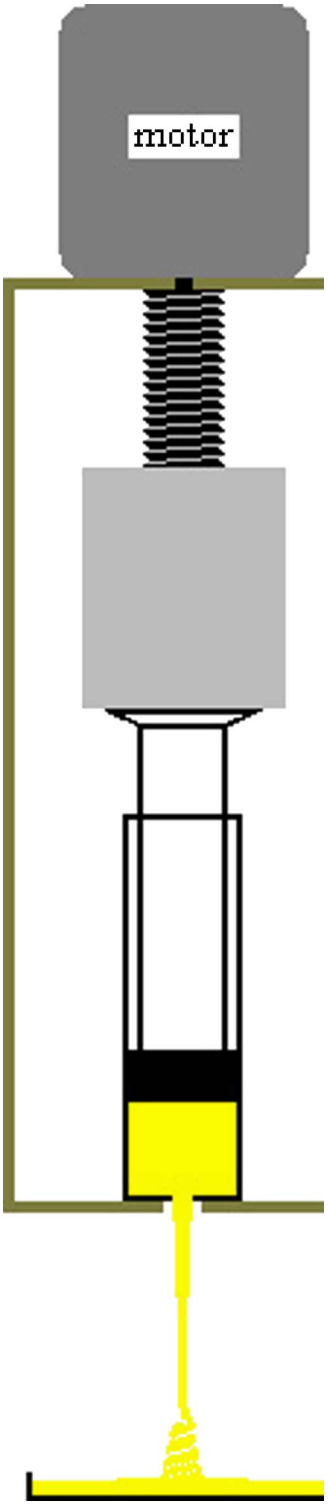

FIG. 1. (Color online) Experimental setup for low frequencies.

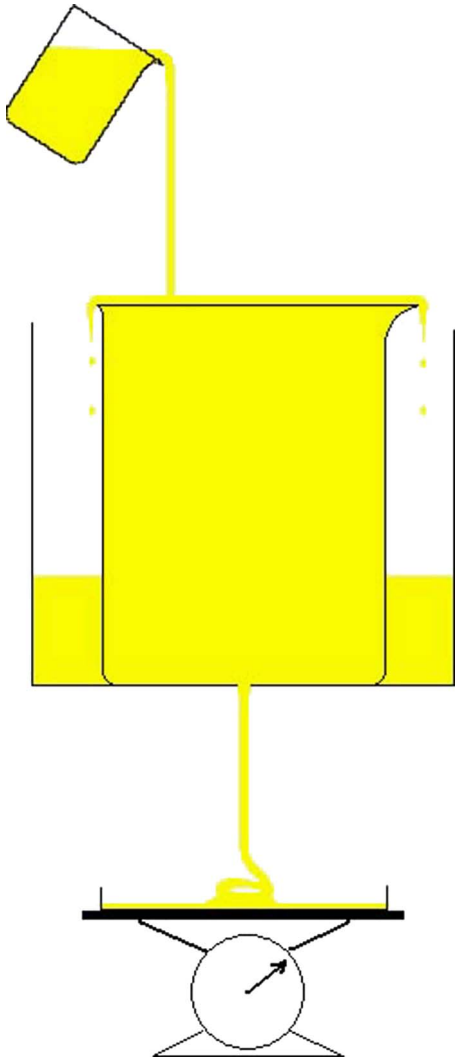

FIG. 2. (Color online) Experimental setup for high frequencies.

with a macro objective and a flash to avoid motion blur.

For both setups, the fall height H was varied using a mechanical jack. The values of H reported below are all effective values, measured from the orifice down to the point where the rope first comes into contact with a previously extruded portion of itself. The effective fall height H is thus the total orifice-to-plate distance less the height of the previously extruded fluid that has piled up beneath the falling rope.

III. STEADY COILING REGIMES

To set the stage for our investigation, we summarize briefly here the four regimes of steady coiling (viscous, gravitational, inertial, and inertio-gravitational) and the experimental evidence for their existence. For convenience, we denote these regimes by the symbols V, G, I, and IG.

The first three regimes (V, G, and I) are defined by the relative magnitudes off the viscous, gravitational, and inertial forces acting on the "coil" portion of the rope, where deformation occurs primarily by bending and twisting (as opposed to stretching). The total viscous (F_V), gravitational (F_G), and inertial (F_I) forces per unit length of the rope are [14,15]

$$F_V \sim \rho \nu a_1^4 U_1 R^{-4}, \quad F_G \sim \rho g a_1^2, \quad F_I \sim \rho a_1^2 U_1^2 R^{-1}, \quad (1)$$

where a_1 is the radius of the rope in the coil, R is the radius of the coil itself, $U_1 \equiv Q/\pi a_1^2$ is the axial velocity of the fluid within the coil, and g is the gravitational acceleration.

In the viscous (V) regime, both gravity and inertia are negligible ($F_G, F_I \ll F_V$), and coiling is driven entirely by fluid extrusion, like the coiling of toothpaste squeezed from a tube. To within a multiplicative constant, the frequency of V coiling is [15]

$$\Omega_V = \frac{Q}{H a_1^2}, \quad (2)$$

which is independent of viscosity because the velocity of the rope is fully determined kinematically by the imposed injection rate. In the gravitational regime, the viscous forces that resist bending are balanced by gravity with negligible inertia ($F_G \approx F_V \gg F_I$), and the coiling frequency scale is [15]

$$\Omega_G = \left(\frac{g Q^3}{\nu a_1^8}\right)^{1/4}. \quad (3)$$

In the inertial regime, gravity is negligible and the viscous forces are balanced by inertia ($F_I \approx F_V \gg F_G$). The corresponding scale for the coiling frequency is [14]

$$\Omega_I = \left(\frac{Q^4}{\nu a_1^{10}}\right)^{1/3}. \quad (4)$$

The frequency scales (2)–(4) all depend strongly on the radius a_1 of the rope within the coil, which in the G and I regimes is much less than the injected radius a_0 because of gravity-induced stretching. Because the parameter a_1 plays such a central role in setting the coiling frequency, we have measured it in all our experiments.

Unlike the first three regimes, the frequency of IG coiling is determined by the balance of forces acting on the long "tail" portion of the rope above the coil, which behaves like a whirling "viscous string" that deforms primarily by stretching. Gravity, centrifugal inertia, and the viscous forces that resist stretching are all important here. Coiling at a fixed height can occur with different frequencies, each of which is proportional to the familiar pendulum frequency

$$\Omega_{\mathrm{IG}} = \left(\frac{g}{H}\right)^{1/2}, \quad (5)$$

with constants of proportionality that depend weakly on the dimensionless parameter $g d^2 H^2/\nu Q$ [10].

Figure 3 shows experimental evidence for the existence of the four coiling regimes discussed above. The V and G regimes appear clearly in Fig. 3(a), which shows the coiling frequency Ω (circles) measured as a function of height in an experiment with $Q = 0.0038\ \mathrm{cm^3\ s^{-1}}$ performed using the low-frequency setup (Fig. 1). The frequency decreases strongly as a function of height for $0.25\ \mathrm{cm} < H < 0.8\ \mathrm{cm}$, and then becomes constant or increases slightly thereafter.

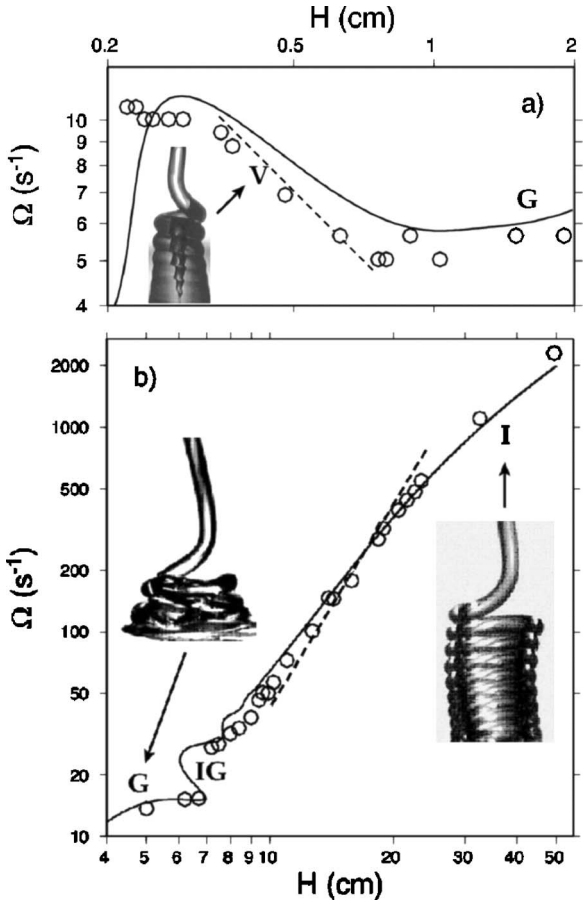

FIG. 3. Curves of angular coiling frequency vs fall height showing the existence of four distinct coiling regimes: Viscous (V), gravitational (G), inertio-gravitational (IG), and inertial (I). Experimental measurements are denoted by circles and numerical calculations based on slender-rope theory [15] by solid lines. Error bars on the experimental measurements of Ω and H are smaller than the diameter of the circles in most cases. The typical appearance of the coiling rope in the V, G, and I regimes is shown by the inset photographs. (a) Slow (inertia-free) coiling with $\nu=100$ cm^2 s^{-1}, $a_0=0.068$ cm, and $Q=0.0038$ cm^3 s^{-1}. The dashed line shows the simplified viscous coiling scaling law (6). (b) Higher-frequency coiling with $\nu=300$ cm^2 s^{-1}, $a_0=0.25$ cm, and $Q=0.094$ cm^3 s^{-1}. The dashed line shows the inertial coiling scaling law (8).

Because gravitational stretching of the rope is negligible ($a_1 \approx a_0$) for 0.25 cm$<H<$0.8 cm, the scaling law (2) for V coiling implies

$$\Omega_V \propto H^{-1}. \tag{6}$$

The scaling law (6) is shown by the dashed line in Fig. 3(a), and agrees well with the experimental measurements for 0.25 cm$<H<$0.8. For comparison, the solid line shows the coiling frequency predicted numerically for the parameters of the experiment, including the effect of surface tension. The trends of the numerical curve and of the experimental data are in good agreement, although the latter are 15–20 % lower on average for unknown reasons. The rapid increase of frequency with height predicted by the numerical model for

FIG. 4. Coexisting coiling states in an experiment with $\nu=300$ cm^2 s^{-1}, $Q=0.041$ cm^3 s^{-1}, $d=0.15$ cm, and $H=4.5$. (a) Low-frequency state; (b) high-frequency state.

$H<0.25$ cm corresponds to coiling states in which the rope is strongly compressed against the plate. We were unable to observe such states because the rope coalesced rapidly with the pool of previously extruded fluid flowing away from it.

The G, I, and IG regimes appear in Fig. 3(b), which show measurements of coiling frequency vs height in an experiment with $\nu=300$ cm^2 s^{-1} and and $Q=0.094$ cm^3 s^{-1} performed using the high-frequency setup (Fig. 2). As the height is increased, the coiling regime evolves from G (4 cm$<H<$6 cm) through IG (6 cm$<H<$8 cm; multivalued) to I ($H>8$ cm). The slope of the curve $\Omega(H)$ for 9 cm$<H<$20 cm can be understood using a simple scaling argument. In this height range, inertia is important in the coil but not in the tail of the rope, where gravity is balanced by the viscous forces that resist stretching. In the limit $a_1 \ll a_0$ corresponding to strong stretching, this force balance implies [15]

$$a_1 \sim (Q\nu/g)^{1/2} H^{-1}, \tag{7}$$

which when combined with Eq. (4) yields

$$\Omega_I \sim H^{10/3}. \tag{8}$$

The scaling law (8) is shown by the dashed line in Fig. 3(b) and is in reasonably good agreement with the experimental measurements. The latter agree still more closely with the full numerical solution (solid line), which includes additional effects such as surface tension that were neglected in the simple scaling analysis leading to Eq. (8). The steady decrease in the slope of $\Omega(H)$ for $H>20$ cm is due to the increasing effect of inertia in the tail of the rope, which inhibits gravitational stretching and increases a_1 relative to the value predicted by Eq. (7).

IV. TIME DEPENDENCE OF INERTIO-GRAVITATIONAL COILING

In the laboratory, coiling in the IG regime is inherently time dependent, taking the form of an aperiodic oscillation between two quasisteady states with different frequencies for a given fall height. Such an oscillation occurs, e.g., at $H \approx 7$ cm in the experiment of Fig. 3(b). The typical appearances of the two quasisteady states are shown (for a different experiment) in Fig. 4. Note first that the coil radius $R \equiv U_1/\Omega$ is always smaller for the state with the higher frequency, because the axial velocity U_1 of the rope being laid down (which depends only on the fall height) is nearly the same for both states. Moreover, the total height of the fluid "pile" beneath the coiling rope is greater for the high-

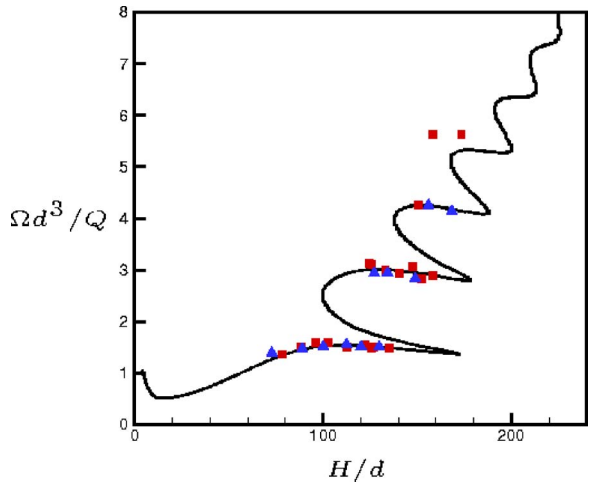

FIG. 5. (Color online) Rescaled coiling frequency as a function of the rescaled fall height, for an experiment performed using the low-frequency setup (Fig. 1) with $\nu=1000$ cm^2 s^{-1}, $d=0.068$ cm, and $Q=0.00258$ cm^3 s^{-1}. Symbols: Experimental measurements obtained with the fall height increasing (squares) and decreasing (triangles). Solid line: Prediction of the slender-rope numerical model.

frequency state. This is because the pile height is controlled by a steady-state balance between two effects: Addition of fluid (the coiling rope) at the top, and removal of fluid at the bottom by gravity-driven coalescence of the pile into the pool of fluid spreading on the plate. Now the coalescence rate increases linearly with the pile height and the rate at which fluid addition builds up the pile ($\equiv Q/4\pi R a_1$) is greater for the high-frequency state. The height of the pile must therefore also be greater for this state.

Paradoxically, the origin of the time dependence of IG coiling is revealed by the curves of $\Omega(H)$ for *steady* coiling. These curves are multivalued in the height range corresponding to the IG regime, implying that two or more steady states

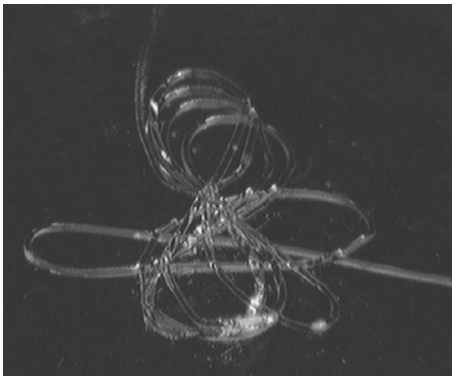

FIG. 6. Intermediate "figure of eight" state for an experiment with $\nu=5000$ cm^3 s^{-1}, $Q=0.00145$ cm^3 s^{-1}, $d=0.068$ cm, and $H=16.5$ cm.

can exist at a fixed fall height [e.g., 6 cm$<H<$8 cm in Fig. 3(b)]. Maleki *et al.* [9] demonstrated that the (numerically predicted) frequencies of these steady states are in fact identical to the frequencies of the two quasisteady states observed in the laboratory.

Here we investigate the time dependence of IG coiling in more detail, focusing on the multiplicity of the coexisting states and the fine structure of the transitions between them. We begin by noting that the multivaluedness of a given curve $\Omega(H)$ can be conveniently characterized by the number N of turning (fold) points it contains. Here we define turning points as points where $d\Omega/dH=\infty$ and $d^2\Omega/dH^2>0$; thus $N=2$ for the solid curve in Fig. 3(b). Ribe *et al.* [16] showed numerically that N is controlled primarily by the value of the dimensionless parameter

$$\Pi_1 = \left(\frac{\nu^5}{gQ^3}\right)^{1/5}, \tag{9}$$

scaling as $N\sim\Pi_1^{5/32}$ in the limit $\Pi_1\to\infty$. The experiment of Fig. 3(b) has $\Pi_1=313$, which is not large enough for the

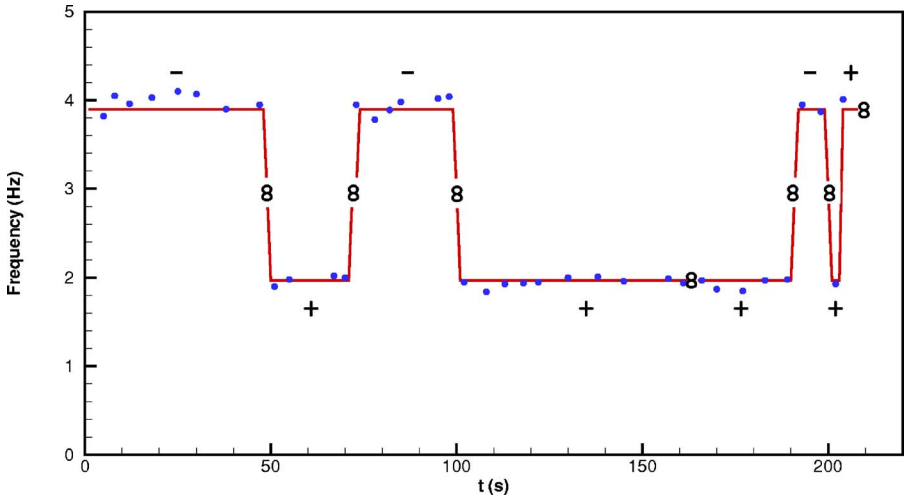

FIG. 7. (Color online) Coiling frequency as a function of time for the experiment of Fig. 5 and $H=8.55$ cm. The experimental measurements are shown by circles and the numerically predicted frequencies for the fall height in question are represented by the horizontal portions of the solid line. The symbol "8" indicates the appearance of an intermediate "figure of eight" state, as described in the text. The "+" and "−" signs indicate counterclockwise and clockwise rotation, respectively. The oscillation shown is between the two lowest "steps" in Fig. 5.

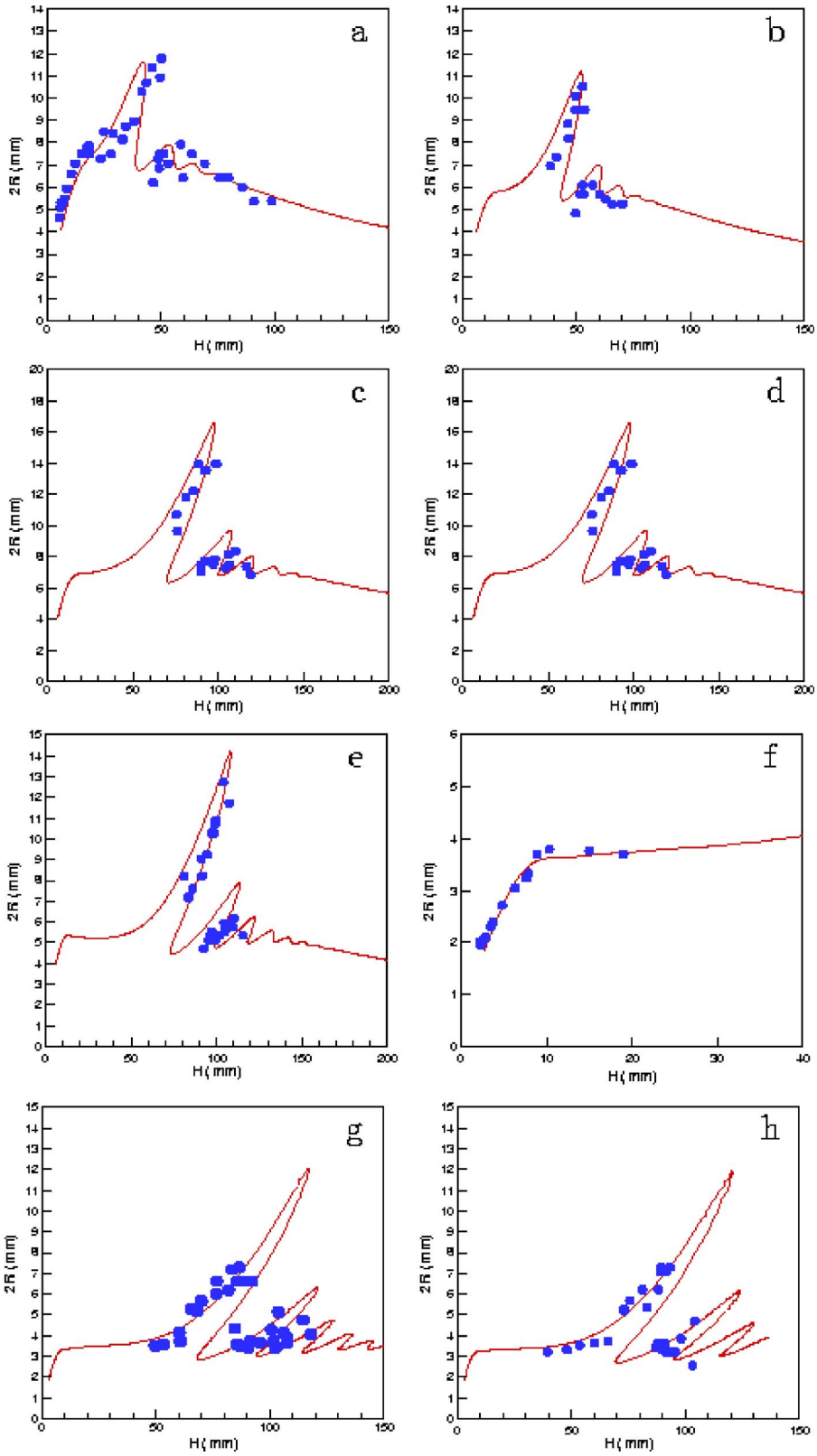

FIG. 8. (Color online) Coil radius R as a function of height for eight experiments with different values of (Π_1, Π_2). (a) (297, 2.8); (b) (465, 2.35); (c) (1200, 2.08); (d) (1742, 2.99); (e) (3695, 2.19); (f) (7143, 3.67); (g) (9011, 3.33); (h) (10052, 3.18). The circles and the solid line show the experimental measurements and the predictions of the slender-rope numerical model, respectively.

multivalued character of $\Omega(H)$ to appear with full clarity. Accordingly, we used our low-frequency setup (Fig. 1) to perform an experiment with $\nu = 1000\ \mathrm{cm}^2\ \mathrm{s}^{-1}$ and a very low flow rate $Q = 0.00258\ \mathrm{cm}^3\ \mathrm{s}^{-1}$, corresponding to $\Pi_1 = 8490$. The numerically predicted $\Omega(H)$ (Fig. 5, solid line) now has $N=6$, with up to seven distinct steady states possible at a fixed fall height ($H/d \approx 170$). The experimental measurements (solid symbols in Fig. 5) group themselves along four distinct branches or "steps" that agree remarkably well with the numerical predictions, except for a small offset at the highest step. To our knowledge, this is the first experimental observation of four distinct steps in IG coiling (three were

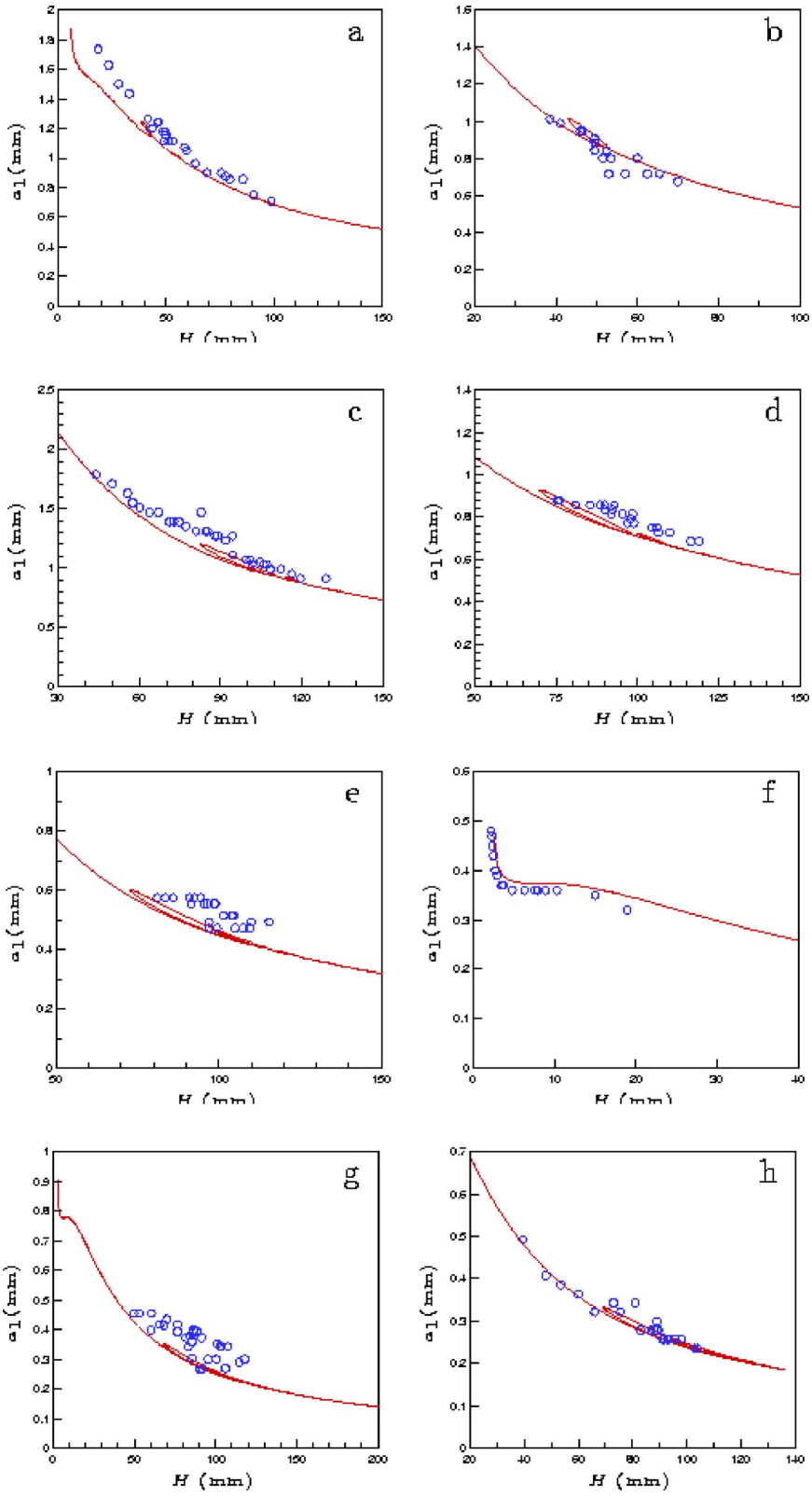

FIG. 9. (Color online) Rope radius a_1 within the coil as a function of height, for the same experiments as in Fig. 8.

seen by [10]). We did not observe any coiling states along the backward-sloping portions of the $\Omega(H)$ connecting the steps, probably because these states are unstable to small perturbations [16].

We turn now from the coexisting states themselves to the transitions between them. These occur spontaneously, and appear to be initiated by small irregularities in the pile of fluid already laid down beneath the coiling rope. In most (but not all) cases, the transition occurs via an intermediate "figure of eight" state, an example of which is shown in Fig. 6. During, e.g., a low- to high-frequency transition, the initially circular coil first changes to a "figure of eight" whose largest

dimension is nearly the same as the diameter of the starting coil. The new, high-frequency coil then forms over one of the loops of the "figure of eight." If the new coil forms over the loop of the "eight" that was laid down first, the sense of rotation (clockwise or counterclockwise) of the new coil is the same as that of the old. If, however, the new coil forms over the second loop, the sense of rotation changes.

Further understanding of the transition can be gained by measuring the coiling frequency and the sense of rotation as a function of time (Fig. 7). The experimental measurements (circles) show a clear oscillation between two states whose frequencies agree closely with the numerically predicted frequencies of steady coiling at the fall height in question (horizontal portions of the solid line). The oscillation is irregular, with no evident characteristic period, in keeping with the hypothesis that transitions are initiated by irregularities in the fluid pile. The only clear trend we were able to observe was that the low-frequency state tends to be preferred when the coiling occurs close to the *G* regime (i.e., for lower heights), while the high-frequency state is preferred near the *I* regime (greater heights). The sense of rotation (indicated by the symbols "+" or "−" in Fig. 7) usually changes during the transition, but not always. All the transitions in Fig. 7 occur via an intermediate "figure of eight" state (indicated by the symbol "8"), but in other experiments we have observed the "figure of eight" without any transition, as well as transitions that occur without any "figure of eight."

V. RADIUS OF THE COIL AND THE ROPE

The expressions (1) show that the forces per unit length acting on the rope depend critically on the radius R of the coil and the radius a_1 of the rope within the coil. Here we present a systematic series of laboratory measurements of R and a_1, and compare them with the predictions of the slender-rope numerical model [15]. Most previous experimental studies of liquid rope coiling have focused on measuring the coiling frequency. Only a few [8,9] have measured the radius a_1 in addition, and none (to our knowledge) has presented measurements of the coil radius R.

The measurements we present here were obtained in eight experiments with different values of ν, d, and Q. For convenience, we characterize each of these experiments by its associated values of the dimensionless parameters Π_1 and Π_2, where Π_1 is defined by Eq. (9) and

$$\Pi_2 = \left(\frac{\nu Q}{g d^4}\right)^{1/4}. \tag{10}$$

Figure 8 shows the coil radius R as a function of the height for the eight experiments. The agreement between the measured values and the numerics (with no adjustable parameters) is very good overall. The coil radius is roughly constant in the *G* regime, which is represented by the relatively flat portions of the numerical curves at the left of panels (b), (c), (d), (e), (g), and (h). The subsequent rapid increase of the coil radius with height corresponds to the beginning of the IG regime. At greater heights within the IG regime, the coil radius exhibits a multivalued character similar to the one we have already seen for the frequency (e.g., Fig. 5).

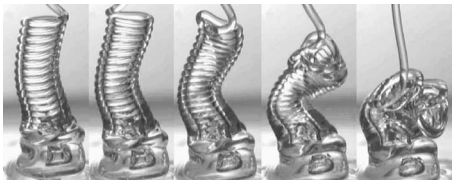

FIG. 10. Secondary buckling of the coil in the inertial regime, in an experiment performed using the high-frequency setup (Fig. 2) with $\nu = 125$ cm^2 s^{-1}, $d = 0.15$ cm, $Q = 0.072$ cm^3 s^{-1}, $H = 14$ cm, and $a_1 = 0.7$ mm. Time between two photographs is nearly 0.1 s.

The structure of the curves $a_1(H)$ (Fig. 9) is much simpler, exhibiting in most cases a monotonic decrease as a function of height that reflects the increasing intensity of gravitational stretching of the falling rope. The only significant departures from the simple structure are the rapid decrease of a_1 as a function of H in the *V* regime [leftmost portions of panels (f) and (g)] and a small degree of multivaluedness in the IG regime. The agreement between the measured values and the numerics is good, although the latter tend to be somewhat lower than the former on average.

VI. SECONDARY BUCKLING

In the high-frequency inertial regime, the rapidly coiling rope can pile up to a great height, forming a hollow fluid column whose length greatly exceeds the rope diameter. When the height of the column exceeds a critical value H_c, it collapses under its own weight (Fig. 10), and the process then repeats itself with a well-defined period that greatly exceeds the coiling period. We call this phenomenon "secondary buckling," as opposed to the "primary" buckling that is responsible for coiling in the first place.

As a first step towards a physical understanding of secondary buckling, we apply dimensional analysis to measurements of the critical height from 13 different laboratory experiments. The critical buckling height H_c can depend on the fluid density ρ, the kinematic viscosity ν, the surface tension coefficient γ, the coil radius R, the rope diameter $d_1 \equiv 2a_1$, and the flow rate Q, or (equivalently) the effective velocity $U_0 \equiv Q/2\pi d_1 R$ at which fluid is added to the top of the column. From these seven parameters four dimensionless groups can be formed, which we take to be

$$G_0 = \frac{H_c}{d_1}, \quad G_1 = \frac{\nu U_0}{g d_1^2}, \quad G_2 = \frac{\gamma}{\rho g d_1^2}, \quad G_3 = \frac{R}{d_1}. \tag{11}$$

The groups G_0, G_1, and G_2 are identical to those used by Yarin and Tchavdarov [17] (henceforth YT96) in their study of the onset of buckling in plane liquid sheets. Buckingham's Π-theorem now implies

$$\frac{H_c}{d_1} = f(G_1, G_2, G_3), \tag{12}$$

where the functional dependence remains to be determined.

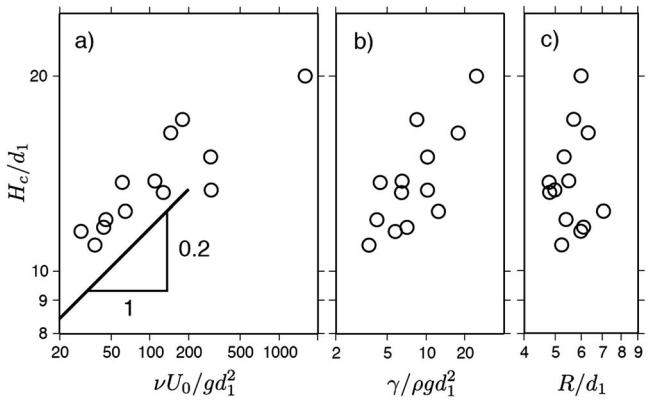

FIG. 11. Critical height H_c for secondary buckling as a function of the dimensionless parameters (a) G_1, (b) G_2, and (c) G_3 defined by Eq. (11). The solid line in part (a) is the critical buckling height predicted by a linear stability analysis for a planar film [17].

Figure 11 shows the measured values of H_c/d_1 for our thirteen experiments as functions of (a) G_1, (b) G_2, and (c) G_3. For comparison, Fig. 11(a) also shows the critical buckling height for plane liquid sheets [17], which is independent of the surface tension for $G_1 > 20$ when $G_2 \leqslant 0.9$ (the largest value of G_2 considered by YT96).

Figure 11(a) shows that the buckling height depends systematically on the dimensionless flow rate G_1. The trend of the data is roughly consistent with the slope $d(\ln H_c)/d(\ln \Pi_1) \approx 0.2$ for a planar film [solid line in Fig. 11(a)], although the heights we observed were about 25% larger. Our observed heights also depend systematically on the inverse Bond number G_2 [Fig. 11(b)]. This dependence has no analog in the case of a planar film, for which the predicted value of H_c at high flow rates is independent of the surface tension [17]. Finally, our measurements show no systematic dependence on the coil radius R [Fig. 11(c)], although we note that the total range of the parameter R/d_1 is less than a factor of 2 in our experiments.

The comparison of our measurements with YT96's theoretical predictions for a planar film must be interpreted with caution for several reasons. First, the geometries are quite different: YT96's steady basic state is a two-dimensional sheet whose thickness becomes infinite at its point of contact with the plate, whereas ours is a cylinder whose wall thickness is everywhere finite. Moreover, the sheets studied by YT96 are clamped at both ends, whereas the upper rim of our cylinder is free to move. A further consequence of this different boundary condition is that surface tension acting on the cylinder's rim exerts an additional downward force that has no analog in the problem studied by YT96. Finally, at high flow rates the theoretical predictions of YT96 are not in good agreement with the laboratory experiments of Cruickshank [3,4], which show that H_c is nearly independent of the flow rate. Clearly, further theoretical work is required to understand the stability of a viscous cylinder with a free upper rim. A study of this problem is currently underway and will be reported separately.

VII. CONCLUSION

We have combined laboratory measurements with numerical modeling to investigate three little-explored aspects of liquid rope coiling: The time dependence of inertio-gravitational coiling, the dependence of the radii of the coil and the rope on the experimental parameters, and the "secondary buckling" of the columnar structure generated by inertial coiling. In the IG regime, we have documented experimentally the existence of four distinct branches of quasisteady coiling states in the frequency-fall height space. Moreover, detailed measurements of the coiling frequency as a function of time demonstrate that the transitions between coexisting states have no characteristic period, may take place with or without a change in the sense of rotation, and usually (but not always) occur via an intermediate "figure of eight" state. We present extensive laboratory measurements of the radii of the coil and of the rope within it and show that they agree well with the predictions of a "slender-rope" numerical model. Finally, we have shown that the critical column height for secondary buckling varies with the flow rate in a way that is consistent with previous results for buckling planar sheets, but that there is an additional dependence on the surface tension that has no analog for a sheet.

ACKNOWLEDGMENTS

This work has been supported by the Center for International Research and Collaboration (ISMO), the French embassy in Tehran, and the DyETI program of INSU (France). We thank P. Moller for helpful discussions and assistance with the experiments. This is IPGP contribution number 2166.

[1] G. Barnes and R. Woodcock, Am. J. Phys. **26**, 205 (1958).
[2] G. Barnes and J. MacKenzie, Am. J. Phys. **27**, 112 (1959).
[3] J. O. Cruickshank, Ph.D. thesis, Iowa State University, 1980.
[4] J. O. Cruickshank and B. R. Munson, J. Fluid Mech. **113**, 221 (1981).
[5] H. E. Huppert, J. Fluid Mech. **173**, 557 (1986).
[6] See EPAPS Document No.E-PLEEE8-74-100612 for movies of the coiling. For more information on EPAPS, see http://www.aip.org/pubservs/epaps.html.
[7] R. W. Griffiths and J. S. Turner, Geophys. J. (Oxford) **95**, 397 (1988).
[8] L. Mahadevan, W. S. Ryu, and A. D. T. Samuel, Nature (London) **392**, 140 (1998).
[9] M. Maleki *et al.*, Phys. Rev. Lett. **93**, 214502 (2004).
[10] N. M. Ribe *et al.*, J. Fluid Mech. **555**, 275 (2006).
[11] G. I. Taylor, *Proceedings of the 12th International Congress of Applied Mechanics* (Berlin, Springer, 1968).
[12] J. O. Cruickshank, J. Fluid Mech. **193**, 111 (1988).

[13] B. Tchavdarov, A. L. Yarin, and S. Radev, J. Fluid Mech. **253**, 593 (1993).
[14] L. Mahadevan, W. S. Ryu, and A. D. T. Samuel, Nature (London) **403**, 502 (2000).
[15] N. M. Ribe, Proc. R. Soc. London, Ser. A **460**, 3223 (2004).
[16] N. M. Ribe, M. Habibi, and D. Bonn Phys. Fluids **18**, 084102 (2006).
[17] A. L. Yarin and B. M. Tchavdarov, J. Fluid Mech. **307**, 85 (1996).